NanoImpact 42 (2026) 100630

Contents lists available at ScienceDirect

NanoImpact

journal homepage: www.elsevier.com/locate/nanoimpact

Research Paper

Antimicrobial nano silver (Ag)-enabled wound dressing evaluated using open flow microperfusion: Comparison of uncoated *versus* hydroxyethyl cellulose-coated Ag

Ilaria Zanoni [a], Simon Schwingenschuh [b], Thomas Birngruber [b], Peter Reisenegger [b], Sandeep Keshavan [c], Sebastian Santhosh Martin [c], Bengt Fadeel [c], Kai Moritz Eder [d], Jürgen Schnekenburger [d], Alessandro Bonetto [e], Elena Badetti [e], Claudia Vineis [f], Simona Ortelli [a], Anna Luisa Costa [a], Magda Blosi [a,*]

[a] CNR-ISSMC, National Research Council of Italy, Institute of Science, Technology and Sustainability for Ceramics, 48018 Faenza, Italy
[b] HEALTH—Institute for Biomedical Research and Technologies, Joanneum Research Forschungsgesellschaft mbH, 8010 Graz, Austria
[c] Institute of Environmental Medicine, Karolinska Institutet, 171 77 Stockholm, Sweden
[d] Biomedical Technology Center, University of Muenster, 48149 Muenster, Germany
[e] DAIS–Department of Environmental Sciences, Informatics and Statistics, University Ca'Foscari of Venice, 30170 Venice-Mestre, Italy
[f] CNR-STIIMA, National Research Council of Italy, Institute of Intelligent Industrial Technologies and Systems for Advanced Manufacturing, Biella, Italy

ARTICLE INFO

Editor: Dr. Bernd Nowack

Keywords:
Ag nanoparticles
Nanobiomaterials
Dermal open flow microperfusion (dOFM)
SSbD-transition
Wound dressing

ABSTRACT

Silver nanoparticles (NPs) are frequently deployed in medical devices due to their antimicrobial properties. We previously reported an eco-friendly process for preparing AgNPs by using a quaternary ammonium salt of hydroxyethyl cellulose (HEC) as a capping and reducing agent. Here, inspired by the Safe and Sustainable by Design framework, we conducted a comprehensive safety and efficacy assessment of AgHEC *versus* commercial uncoated AgNPs before and after their integration into wound dressings based on poly L-lactic acid fibers prepared by electrospinning (PLLA-Ag and PLLA-AgHEC). We demonstrated that the AgHEC formulation displayed an improved antibacterial efficacy compared to its uncoated counterpart. We also performed colloidal and dissolution studies *in vitro* using relevant biological media. Moreover, the toxicological evaluation using state-of-the-art porcine skin models and the clinically relevant dermal open flow microperfusion (dOFM) approach demonstrated negligible penetration of silver through both intact and disrupted skin while no evidence for elevated inflammatory immune responses was noted compared to the control. Taken together, our findings not only validate AgHEC as an alternative for wound healing applications but also establishes a robust methodological framework for the future evaluation of other nanobiomaterials.

1. Introduction

Owing to their well-established antimicrobial activity, silver nanoparticles (AgNPs) are frequently incorporated into biomedical devices such as catheters, implant coatings, and medical bandages. In wound care specifically, the challenge of microbial resistance in chronic wounds makes AgNPs a particularly valuable antimicrobial agent. Silver-based dressings are a key component in the treatment of pathological wounds, including diabetic foot ulcers, pressure ulcers, and burns (Shi et al., 2020; Paladini and Pollini, 2019; Cazzagon et al., 2022). Beyond their broad-spectrum antimicrobial efficacy in controlling bioburden and biofilm, these dressings actively promote healing by driving fibroblast differentiation, keratinocyte proliferation, and wound contraction (Ciofu et al., 2017; Percival and McCarty, 2015), offering a superior therapeutic profile compared to alternatives such as calcium alginate (Jude et al., 2007). By providing a moist healing environment, managing exudate, and serving as an antimicrobial barrier, Ag-based dressings fulfill many of the requirements for an ideal dressing that mimics the natural extracellular matrix (Cassa et al., 2024; Dhivya et al., 2015). Moreover, AgNPs do not provoke the development of resistance in bacteria (Wu et al., 2022).

Despite the clear therapeutic benefits, Ag-based dressings face

* Corresponding author.
E-mail address: magda.blosi@issmc.cnr.it (M. Blosi).

https://doi.org/10.1016/j.impact.2026.100630
Received 8 January 2026; Received in revised form 27 April 2026; Accepted 27 April 2026
Available online 28 April 2026

critical safety concerns. While the release of dissolved silver ions is often suggested as the primary cause of toxicity, clear evidence indicates that ion release alone cannot account for all observed toxic effects (Albalghiti et al., 2021; Paladini and Pollini, 2019). The major safety risk is the potential for particle penetration into the damaged skin or tissues, which remains a significant concern for human toxicity (Crosera et al., 2009; Larese Filon et al., 2015; Maeda et al., 2025; Tak et al., 2015). Once AgNPs penetrate the damaged barrier, they can act as a "Trojan horse," migrating deeper and subsequently releasing ions into systemic circulation (Larese Filon et al., 2009). For this reason, a strategic material design that balances penetration and antibacterial properties is needed (Paladini and Pollini, 2019). The development of intrinsically safer and more sustainable materials is a pivotal goal for the nanotechnology community (Furxhi et al., 2024; Furxhi et al., 2022). The Safe-and-Sustainable-by-Design (SSbD) framework formulated by the European Commission's Joint Research Centre (JRC) (Caldeira et al., 2022) mandates that safety and sustainability must be integrated from the earliest stages of chemical and material innovation (Caldeira et al., 2024; Garmendia Aguirre et al., 2025).

The EU-funded BIORIMA (Biomaterials Risk Management) consortium sought to develop a risk management framework for nanobiomaterials (NBMs) used in medical devices and advanced therapy medicinal products (ATMPs) (Giubilato et al., 2020). Here, as a case study on NBMs, we evaluated AgNPs coated with hydroxyethyl cellulose (AgHEC) as an SbD alternative to conventional AgNPs for use in wound dressings. AgHEC was compared with commercial uncoated AgNPs before and after incorporation into poly L-lactic acid fibers (PLLA-Ag and PLLA-AgHEC), constituting the wound dressing core. In the perspective of considering sustainability metrics within the SbD approach, we selected AgHEC as it was prepared through an eco-friendly, highly transferable, and patented synthesis (Costa and Blosi, 2016), previously validated by a multi-criteria decision analysis algorithm which integrated performance with Life Cycle Assessment (LCA) and Life Cycle Costing (LCC) (Blosi et al., 2024). Moreover, the HEC coating is a quaternary ammonium salt of hydroxyethyl cellulose (HEC) and low-toxic reagent, with intrinsic antimicrobial properties and promotes the achievement of concentrated AgHEC suspensions with excellent efficacy against pathogenic strains and viruses (Costa et al., 2022; Marassi et al., 2018).

In the perspective of collecting preliminary data for the implementation of the SSbD framework, this study initiates the innovation process by focusing on the Safety and Functionality pillars. While no specific quantitative calculations for a full assessment were performed, the results may provide an experimental basis for a tailored hazard characterization for a Safety Assessment during use. To this end, a multi-tiered characterization was applied, providing physicochemical, functional, and toxicological data relevant to the wound dressing's use stage as a fundamental starting point for a full SSbD assessment (Fig. 1).

This included colloidal and dissolution studies in relevant biological media, antimicrobial activity evaluation, and safety assessment through dermal open flow microperfusion (dOFM). dOFM is an innovative, clinically approved technology to investigate the pharmacokinetics (PK) and pharmacodynamics (PD) of NBMs in the skin (Birngruber et al., 2022; Bodenlenz et al., 2017). Two complementary porcine models supported by dOFM were applied, an *ex vivo* model to quantify penetration through the skin barrier, and an *in vivo* model to characterize the inflammatory response triggered by intradermal delivery, providing important insights regarding the safety of the NBMs.

2. Materials and methods

2.1. Chemicals and materials

Ag nanoparticles (catalogue no. 484059) were purchased from Sigma-Aldrich (Milan, Italy), while coated AgHEC NPs were synthesized following the patented procedure at CNR-ISSMC (Costa and Blosi, 2016). Polyquaternium-67 polymer SoftCAT SL, the cationic quaternized hydroxyethylcellulose compound, was provided by Dow Chemical (Midland, MI, USA). Synthetic sweat was prepared by mixing NaCl (0.5% wt), lactic acid (0.1% wt), and urea (0.1% wt), pH was corrected to 4.5 with ammonium hydroxide (1 N). Dulbecco's Modified Eagle Medium (DMEM) supplemented with 10% of fetal bovine serum (FBS) was selected as a representative cell medium for the toxicological testing. All the chemicals used in the dissolution test were provided by Sigma-Aldrich (Milan, Italy). ELO-MEL® isoton (Fresenius Kabi Austria, Graz, Austria) was used as an isotonic solution (refer to Table S1 for composition). Human serum albumin at 200 g/L was provided by Kedrion S.p.A. (Kedrion Biopharma Human albumin 200 g/L, Kedrion S.p.A., Italy). Ultra-pure water was produced by a MilliQ® water purifier system (Millipore, resistivity ≥18.2 MΩ·cm, total organic carbon ≤3 μg/

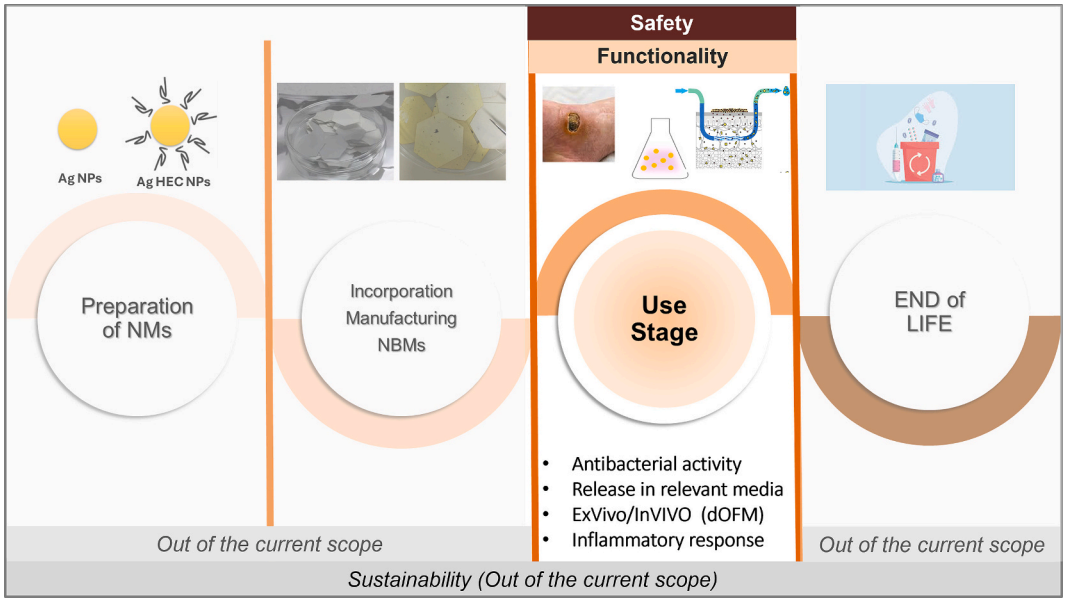

Fig. 1. Methodological roadmap of the study within the SSbD framework, highlighting the focus on Safety and Functionality pillars during the Use stage of Ag-based wound dressings.

L).

2.2. Nanobiomaterials (NBMs)

2.2.1. Silver nanoparticle suspensions

Ag NPs (code 484059, Sigma-Aldrich) suspension, used as reference material, was prepared according to the NANOGENOTOX dispersion protocol (Booth and Alstrup Jensen, 2015; Jensen, 2014; OECD, 2002), obtaining a suspension at 2560 mg/L. AgHEC synthesis was obtained by reducing a solution of $AgNO_3$ at room temperature by means of hydroxyethyl cellulose (HEC) which acts as a capping agent as well. The synthesis procedure provides Ag HEC NPs as a stock suspension with a metallic silver concentration of 0.5% wt. Details on the synthesis of AgHEC were reported previously (Blosi et al., 2024; Costa et al., 2022; Costa and Blosi, 2016).

2.2.2. Endotoxin content

The Limulus Amoebocyte Lysate (LAL) assay was applied to detect bacterial endotoxin contamination as described earlier (Eder et al., 2022; Martin et al., 2022). The Limulus Amoebocyte Lysate PYROTELL®–T assay was purchased from Associates of Cape Cod, Inc. (ACC, East Falmouth, MA) and used according to the manufacturer's instructions with an automated and 37 °C temperature-controlled 660 nm PYROS Kinetix® Flex Tube Reader, (ACC). Data analysis was performed using PYROS® Software (Associates of Cape Cod, Inc.). The prepared Ag-based suspensions were analyzed to assess the endotoxin content by using the LAL assay. LAL assay determined a sterile test if endotoxin levels were < 3 EU/mL.

2.2.3. Nanosilver-enabled wound dressings

The poly L-lactic acid (PLLA) based, nanosilver-enabled wound dressings were obtained by electrospinning technology and were provided by The Electrospinning Company (Harwell, United Kingdom). The preparation protocol involved the addition of Ag NBMs (both uncoated Ag and AgHEC) to the polymeric viscous suspension at a weight concentration of 4% and 5% (*w*/w relative to the polymer), respectively.

2.2.4. Perfusate containing NBMs

ELO-MEL® isoton (a chloride-reduced, acetate-buffered balanced crystalloid) was added to the NBMs (Table S2). The perfusates were prepared by dispersing NBMs evenly in the stock suspensions using a probe sonicator (UP50H, Hielscher Ultrasonics GmbH, Germany), followed by further dilution. Prior to the experiment, the finished test perfusates were sonicated for at least 15 min before being filled into the perfusate reservoir.

2.2.5. Morphological characterization

The morphology and dimension of Ag NPs were evaluated by transmission electron microscopy (TEM) (FEI Tecnai F20). To this end, Ag suspensions diluted at 0.005% wt were drop-casted on a holey carbon film supported by a gold grid. The specimens were then dried at 50 °C to remove the solvent. TEM images were collected in phase contrast mode and by means of selected area electron diffraction (SAED) operating at 200 keV. To gather information about particles morphology the images were taken in phase contrast mode and high-angle annular dark-field scanning transmission mode (HAADF-STEM) (FEI Tecnai F20). The grids were analyzed by TEM and evaluated using an automated image analysis (ImageJ Software V1.53). PLLA fibers were investigated by a field emission scanning electron microscope (FESEM) (Carl Zeiss Sigma NTS, Gmbh Oberkochen, Germany), after coating the spheres with a 5 nm layer of gold.

2.2.6. Colloidal characterization

The colloidal characterization was performed by evaluating the hydrodynamic diameter and zeta potential (ZP) of the Ag NPs diluted in relevant media and by means of three consecutive analyses in triplicate. Synthetic sweat and DMEM +10%FBS (10 and 50 mg/L) were identified as relevant media for the use stage. Samples were exposed to synthetic sweat at 32 °C (mean skin temperature) and data were collected after 1 and 24 h of exposure. The measurements were carried out using dynamic and electrophoretic light scattering (Zetasizer Nano instrument ZSP, ZEN5600, Malvern, UK). The Smoluchowski equation was applied to convert the electrophoretic mobility values to ζ potential values (ZP).

2.2.7. Static particle dissolution

Static dissolution measurements were performed to assess the release during the use phase in different relevant media of Ag^+ from both Ag NPs and nano-enabled products. The release was expressed as the percentage of dissolved Ag^+ relative to the total silver weight (Ag^+/Ag total). Stock suspensions of Ag NPs were prepared in ultrapure water at a concentration of 256 mg/L and further diluted into the relevant media at concentrations of 10 and 50 mg/L. These samples were incubated in synthetic sweat at 32 °C and in DMEM +10% FBS at 37 °C for 1 and 24 h under static conditions. Following exposure, the samples were filtered through 10 kDa cut-off membranes (4200 rpm for 45 min). The filtrated solution was subjected to elemental analysis using ICP-OES technique (Agilent 5100 vertical dual view apparatus Agilent Technologies, Santa Clara, CA, USA). The ICP-OES analysis was performed in radial viewing mode. Calibration curves were established using Ag standards at concentrations of 0.05, 0.1, 1, 10, and 100 mg/L which showed a good correlation ($R^2 > 0.99$). Both standards and diluted samples were acidified with nitric acid (1:10 *v*/v). The concentration of Ag^+ into the media was directly evaluated by ICP-OES determination, with results reported as the average of three independent measurements with relative standard deviation (RSD) %. Next, Ag release from PLLA-Ag and PLLA-AgHEC nano-enabled wound dressings (dimensions of 5.6 cm^2) was investigated in relevant medium consistent with the use-stage conditions for wound dressings: ultrapure water (22 °C, pH = 7 ± 0.1) and synthetic sweat (32 °C, pH = 4.4 ± 0.1). The samples were weighed and immersed in 7 mL of each medium. The amount of Ag released in the media was measured by ICP-OES.

2.3. Antimicrobial activity

The antibacterial activity of AgNPs and PLLA-Ag-based samples was evaluated against Gram-negative bacteria according to ASTM E 2149–2013 "Standard test method for determining the antimicrobial activity of immobilized antimicrobial agents under dynamic contact conditions". The method is used to evaluate the antimicrobial activity of treated specimens under dynamic contact conditions. The applied bacteria are *Escherichia coli* ATCC 11229. The incubated test culture was diluted to give a concentration of 1.5–3.0 × 10^5 CFU/mL (working dilution). This bacterial inoculum was placed in contact with each sample under shaking at room temperature for 1 h using an inoculum ratio of 1 g: 50 mL. All flasks were shaken for 1 h at 190 rpm. After a series of dilutions, 1 mL of the solution was plated on nutrient agar. The inoculated plates were incubated at 37 °C for 24 h and surviving cells were counted.

The antibacterial activity is expressed as the percentage of bacterial reduction based on contact with the test specimen, compared to the number of bacterial cells that survive after contact with the control. It is calculated using Eq. (1):

$$\%\text{reduction}\left(\text{CFU ml}^{-1}\right) = \frac{B - A}{B} \times 100 \quad (1)$$

Here, A is CFU/mL after contact (end test), and B is CFU/mL at zero contact time (used as reference).

Each result is an average of three independent measurements.

2.4. Dermal open flow microperfusion (dOFM)

Dermal open flow microperfusion (dOFM) is a minimally invasive,

probe-based technology that allows continuous sampling of interstitial fluid (ISF) in the dermal layer of the skin (*e.g.*, (Chaturvedi and Garg, 2021; Pieber et al., 2013)). In short, dOFM probes are made of polyether ether ketone (PEEK MS0200600) with an outer diameter of 0.55 mm and a 15-mm-long exchange area with macroscopic openings. dOFM probes were implanted into the skin with the exchange surface positioned in the dermis (Fig. 2). After implantation, the dOFM probes were flushed with OFM perfusate at a flow rate of 10 µL/min for 10 min. The flow rate was then reduced to 1 µL/min. Two different OFM perfusates were used, an isotonic solution (ELO-MEL® isoton) with 1% human serum albumin in the *ex vivo* model and ELO-MEL® isoton only in the *in vivo* model. Two configurations were used to advance the characterization, as depicted in the figure below: topical application of PLLA-Ag and PLLA-AgHEC fibers to the skin (Fig. 2a) and intradermal application of AgNPs and AgHEC suspension *via* perfusion (Fig. 2b).

2.4.1. Ex vivo model

The *ex vivo* model was used to investigate the diffusive skin penetration of Ag NPs and AgHEC NPs after topical application *via* nanosilver-enabled wound dressings (PLLA-Ag or PLLA-AgHEC, on both intact and disrupted skin barriers. Porcine skin (from the flanks about 15 × 50 cm) was explanted postmortem from the back of three domestic pigs (33 ± 3 kg, Table S4) at the Division of Biomedical Research, Medical University of Graz, Austria. Immediately after explantation, the porcine skin was placed in a climate chamber with feedback-controlled temperature and relative humidity (32 °C and 50%). We divided each porcine skin explant into two pieces, one for intact skin and one for skin with a disrupted skin barrier. To disrupt the skin barrier, we removed the stratum corneum *via* tape stripping. Tape stripping was repeated 80–120 times, each time using a fresh piece of adhesive tape (Leukoplast Waterproof, BSN medical GmbH, Germany) and alternating the stripping direction from left to right and right to left. For each skin type (intact or disrupted), PLLA-Ag and PLLA-AgHEC were tested four times, with three applications for dOFM and one for biopsy (Figs. S2). After dOFM implantation and two hours of dOFM baseline sampling, 50 µL of artificial sweat (0.9% wt NaCl in water) were applied and 4 pieces of either PLLA-Ag or PLLA-AgHEC were attached on each skin type using an adhesive film (Opsite Flexifix Transparent Film Roll, Smith & Nephew plc, United Kingdom). After topical application, dOFM samples were collected every two hours for 24 h (Fig. S3) and then biopsies were taken. Before taking the biopsies, the epidermis of the intact skin was removed by heat separation and stored for further analysis, while disrupted skin was only cleaned with gauze pads. 6 mm biopsy punches (pfm medical, Cologne, Germany) were taken and the subcutaneous tissue of the biopsies was removed. All samples were immediately stored at −15 °C to −30 °C and at the end of the experiment, all samples were transferred to −65 to −90 °C until analysis. At the end of the experiment, dOFM probe depths (1.2 ± 0.2 mm ($n = 36$)) were measured using the high-frequency ultrasound LOGIQ and R6 (GE Healthcare, United Kingdom). The amount of Ag in dOFM and biopsies was measured by ICP-MS as reported in section 2.4.4.

2.4.2. In vivo model

The immune response in the dermal layer of the skin was investigated after intradermal delivery of two NPs (Ag and AgHEC NPs) in an *in vivo* pig model by using dOFM for NP delivery and sampling. To successfully deliver NPs into the dermis *via* dOFM, the adsorption of Ag and AgHEC onto the relevant dOFM material (dOFM probe, tubing material, reservoir of perfusate) was tested prior to the *in vivo* model (supplement). The *in vivo* model was conducted using four female domestic pigs (35 ± 8 kg, Table S5). All animal experiments were approved by the Austrian federal government (2020–0.547.803) and performed according to Directive 2010/63/EU on the protection of animals used for scientific purposes. After anesthetizing the pigs (Supplementary Information), three dOFM probes were implanted in the dermis at each of three test sites per pig: one site for Ag NPs, one site for AgHEC NPs, and one control site (no NPs) (Fig. S5). After implantation of the dOFM probe, dOFM was performed at a flow rate of 1 µL/min with a standard perfusate (ELO-MEL® isoton) for 20 min. Then, for intradermal delivery of the NPs, dOFM probes were switched to three different perfusates: standard perfusate with Ag NPs (9 µg/mL); standard perfusate with AgHEC NPs (9 µg/mL); standard perfusate with no NPs at control sites. Prior to switching, the perfusates were sonicated for a minimum of 15 min using a probe sonicator (UP50H, Hielscher Ultrasonics GmbH, Germany). After 40 min the switched perfusate had reached the exchange area of the dOFM probe implanted in the dermis. This marked the start of 12 h of simultaneous dOFM delivery and sampling. Each sampling interval lasted for 4 h. For each site, the sample fluid from the 3 dOFM probes was pooled. At the end of the study, dOFM probe depths (1.4 ± 0.3 mm ($n = 36$)) were measured using the high-frequency ultrasound LOGIQ and R6 (GE Healthcare, United Kingdom). Six skin punch biopsies were taken per test site. Three biopsies were taken at a distance of 0 mm between the dOFM probe and the center of the biopsy and three biopsies were taken at a distance of 2 mm (Fig. S6). The subcutaneous tissue was removed from the biopsies, and the dermal biopsies were pooled according to their test site. All samples were immediately stored at −15 °C to −30 °C and at the end of the experiment all samples were transferred to −65 to −90 °C until analysis. The amount of Ag in dOFM and biopsies was measured as reported in section 2.4.4.

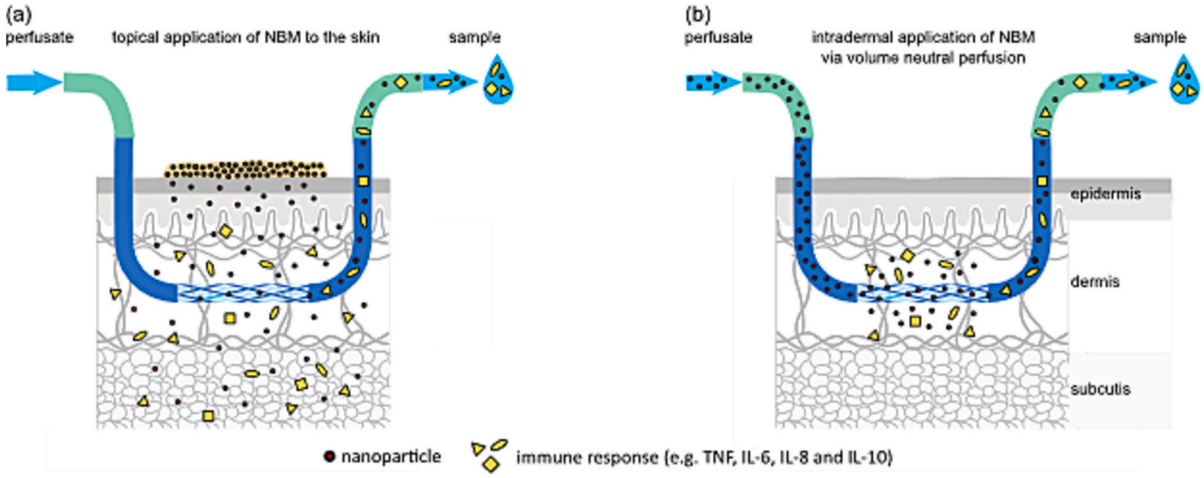

Fig. 2. (a) Working principle of dOFM sampling after topical application of nanosilver-enabled wound dressing. (b) Working principle of the volume-neutral, intradermal delivery of NBMs and simultaneous interstitial fluid sample collection using dOFM to investigate the skin's immune response (cytokine secretion).

2.4.3. Cytokine production

Proinflammatory cytokines were measured by using porcine sandwich ELISA (enzyme-linked immunosorbent assay) kits for tumor necrosis factor (TNF)-α (catalogue no. KSC3011), interleukin (IL)-6 (catalogue no. ESIL6), interleukin (IL)-8 (catalogue no. KSC0081), and interleukin (IL)-10 (catalogue no. KSC0101) (Invitrogen) according to the manufacturer's instructions. The samples were collected from 4 animals (refer to section 2.4.2).

2.4.4. Silver quantification in porcine model

Ag analysis was performed by means of an ICP-MS (Perkin Elmer, Nexion 350XX) coupled with a seaFAST autosampler (direct mode, 4 mL, x10). The Ag (mass 109) was quantified in KED mode (Kinetic Energy Discrimination, 4.4 mL/min) using an external eight-point calibration curve in the range of 0.05–100 μg/L. Instrumental drift was corrected using Rh (103) as the internal standard. For Ag quantification in biopsies, each specimen was lyophilized (Edwards Freeze dryer Modulyo), weighted (Practum, Sartorius, 0.01 mg), and mineralized using 6 mL of H_2O_2:HNO_3 (1:2) mixture. Digestion was performed by using an Ethos Up microwave oven (Milestone) following the "lyophilized meat" program (temperature ramp from room temperature to 210 °C in 20 min, followed by a 15 min hold at 210 °C). The digests were subsequently diluted to a final volume of 50 mL with ultrapure water and analyzed by ICP-MS as previously described. For Ag quantification in dOFM samples (both *in vivo* and *ex vivo*), 0.2 mL of each specimen was treated overnight with 2 mL of an H_2O_2:HNO_3 (1:2) mixture and subsequently diluted to a final volume of 10 mL. These samples were analyzed by ICP-MS as previously described.

2.4.5. Statistical analysis

The area under the curve (AUC) was calculated at 4 h intervals using the linear trapezoidal rule (Gabrielsson and Weiner, 2012). Data were tested for normal distribution using the Shapiro-Wilk test. For normally distributed data, unpaired *t*-tests or one-way ANOVA were applied. For the analysis of the cytokine data described in section 2.4.3, two-way ANOVA was applied. Log-distributed data were log-transformed prior to analysis. Unless otherwise stated, results are presented as mean values ± standard deviation. All statistical tests were performed in GraphPad Prism version 10.5.0 for Windows (GraphPad Software, Boston, MA, USA).

3. Results and discussion

3.1. Nanoparticle characterization

To evaluate the efficacy, safety, and functionality of Ag-based wound dressings, we compared conventional uncoated AgNPs with an SbD alternative, Ag-HEC (AgNPs coated with hydroxyethyl cellulose). A comparative assessment was conducted for the active NPs and the final fibrous dressing in which they were embedded. To support the evaluation of hazard, functionality and exposure potential during the use stage, we implemented a multi-tiered approach involving physicochemical characterization, colloidal behavior in relevant fluids, antibacterial activity, and inflammatory responses using *in vivo* and *ex vivo* models (Fig. 2).

3.1.1. Morphology and colloidal stability

We first investigated the intrinsic properties of the uncoated AgNPs and the AgHEC. TEM images revealed a spherical shape for both Ag-based NPs (Fig. 3). AgNPs showed a diameter in the 30–200 nm range, in agreement with the producer's technical datasheet (Ø DLS: 347 ± 35 nm). AgHEC highlighted smaller dimensions, in the 10–20 nm range, consistent with the applied low-temperature green process (Fig. 3).The endotoxin content assessed by the LAL assay showed endotoxin levels <1 EU/mL for AgNPs and < 1 EU/mL for AgHEC.

The colloidal behavior of uncoated silver nanoparticles (AgNPs) and hydroxyethylcellulose-coated silver (AgHEC) was assessed in ultrapure water, synthetic sweat, and complete cell culture medium (DMEM +10% FBS), with key parameters summarized in Table 1. In ultrapure water, AgNPs formed large aggregates (hydrodynamic diameter: 500–1500 nm), a phenomenon attributed to the precipitation of dry powders from high-temperature processes. The addition of bovine serum albumin (BSA) as a dispersant induced a negative ζ potential (ZP). AgHEC exhibited diameters larger than the real ones assessed by TEM (Marassi et al., 2018) due to the steric hindrance of the HEC polymer, which also conferred a positive ZP. When transferred to physiologically relevant media, both materials responded to the higher ionic strength. AgNPs exhibited significant particle coarsening and a decreased ZP in both synthetic sweat and DMEM+FBS. The aggregation was most pronounced in synthetic sweat, which lacks stabilizing agents. In DMEM+FBS, the ZP stabilized at approximately −10 mV consistent with the formation of a protein corona from the fetal bovine serum (Doorley and Payne, 2011), which provides steric stabilization but resulted in higher polydisperse suspensions (PDI > 0.5).

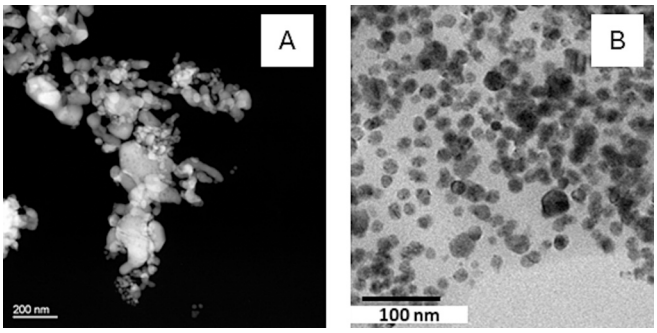

Fig. 3. TEM images of (A) AgNPs, naked nanoparticles and (B) AgHEC. Scale bars: 200 nm (A), 100 nm (B).

For AgHEC, the positive ZP measured in water was neutralized in synthetic sweat due to electric double-layer compression. However, the hydrodynamic diameter remained unchanged, demonstrating that the steric stabilization from HEC prevails over electrostatic contributions. In DMEM+FBS, AgHEC underwent a more complex transformation: an abrupt decrease in particle size was observed alongside a shift to a negative ZP. This suggests that serum components partially replaced or altered the HEC coating, forming new, smaller, and highly stable kinetic units, as confirmed by low PDI values. The stability of both AgHEC suspensions was further corroborated by a distinct surface plasmon resonance band centered at 410 nm (Blosi et al., 2024; Costa et al., 2022).

3.1.2. Silver release in simulated biological environments

To provide a baseline reference for the intrinsic dissolution of the nanoparticles, the release in pure water was also measured (Table 1). AgHEC showed a higher dissolution in water compared to uncoated AgNPs (0.2 mg/L *vs.* 0.02 mg/L after 24 h at 10 mg/L). This can be attributed to the hydrophilic and cationic nature of the quaternized HEC coating, which enhances the dispersibility of the silver core and prevents aggregation, maintaining a higher effective surface area for ion release even in a non-complex medium. In contrast, uncoated AgNPs tend to undergo faster agglomeration in pure water, limiting their surface exposure. The release of Ag^+ ions from AgNPs and AgHEC was then quantified in synthetic sweat and DMEM+FBS (Table 1), and the results showed for AgHEC a slightly lower release than uncoated AgNPs, particularly in DMEM+FBS at lower dose. As expected, the chemical composition of the medium significantly influenced the ion release (Von Goetz et al., 2013; Yetisen et al., 2016). Notably, while uncoated AgNPs always showed higher dissolution in both complex media compared to water, AgHEC exhibited a decrease in solubility in DMEM+FBS even relative to pure water (0.07 mg/L *vs* 0.2 mg/L at 10 mg/L). This suggests

Table 1
Colloidal behavior and dissolution results collected for naked Ag NPs and AgHEC in relevant media (ultrapure water, synthetic sweat, and DMEM + FBS) for two concentrations (10 and 50 mg/L) at two time points (1 and 24 h).

NBMs	Medium	Conc. (mg/L)	Time (h)	Hydrodynamic Size (nm)	PDI	ZP (mV)	pH	%release Ag^+/Ag_{tot}	Ag^+ release (mg/L)
Ag NPs	Water*	10	24	1356 ± 478	0.8	20.6 ± 1.5	6.8	0.27 ± 0.09	0.02 ± 0.01
	Water	50	1	497 ± 32	0.4	26.8 ± 0.5	6.7	–	–
	Synthetic Sweat	10	1	595 ± 66	0.5	20.6 ± 1.5	4.4	4.8 ± 0.7	0.48 ± 0.07
	Synthetic Sweat	10	24	1354 ± 44	0.8	18.2 ± 1.7	4.4	5.1 ± 0.8	0.50 ± 0.08
	Synthetic Sweat	50	1	1164 ± 19	0.6	28.0 ± 0.5	4.5	0.8 ± 0.1	0.40 ± 0.05
	Synthetic Sweat	50	24	1223 ± 30	0.7	20.9 ± 1.8	4.7	1.0 ± 0.1	0.50 ± 0.05
	DMEM + FBS	10	1	569 ± 114	0.7	−8.8 ± 0.7	7.9	1.7 ± 0.5	0.17 ± 0.05
	DMEM + FBS	10	24	1799 ± 77	1	10.1 ± 1.1	8.2	1.9 ± 0.3	0.19 ± 0.03
	DMEM + FBS	50	1	799 ± 2	0.6	11.3 ± 1.2	7.9	0.18 ± 0.03	0.09 ± 0.01
	DMEM + FBS	50	24	684 ± 178	0.7	−9.1 ± 0.7	8.2	0.22 ± 0.03	0.11 ± 0.01
AgHEC	Water	10	1	250 ± 3	0.3	11.2 ± 0.5	na	na	Na
	Water*	10	24	216 ± 5	0.3	9.4 ± 0.4	7.3	2.35 ± 0.04	0.20 ± 0.01
	Water	50	1	418 ± 10	0.5	21.5 ± 0.2	na	na	Na
	Water	50	24	595 ± 24	0.5	11.5 ± 0.7	na	na	Na
	Synthetic Sweat	10	1	176 ± 3	0.3	4.8 ± 0.4	4.5	6.2 ± 0.9	0.62 ± 0.09
	Synthetic Sweat	10	24	253 ± 4	0.3	4.8 ± 0.4	4.5	4.3 ± 0.6	0.43 ± 0.06
	Synthetic Sweat	50	1	266 ± 6	0.3	5.6 ± 0.7	4.8	0.9 ± 0.1	0.45 ± 0.05
	Synthetic Sweat	50	24	267 ± 9	0.3	5.3 ± 0.4	4.8	0.6 ± 0.1	0.30 ± 0.05
	DMEM + FBS	10	1	66 ± 2	0.4	−3.3 ± 0.3	8.4	0.8 ± 0.1	0.08 ± 0.01
	DMEM + FBS	10	24	61 ± 1	0.4	−5.2 ± 0.3	8.7	0.7 ± 0.1	0.07 ± 0.01
	DMEM + FBS	50	1	93 ± 3	0.6	−1.9 ± 0.5	8.5	0.2 ± 0.1	0.10 ± 0.05
	DMEM + FBS	50	24	69 ± 1	0.5	−1.7 ± 0.6	8.7	0.2 ± 0.1	0.10 ± 0.05

na = data not available; *: baseline conditions.

that the complexity of the biological medium, particularly the presence of proteins (FBS), exerts a stabilizing or sequestering effect specifically on the HEC-coated surface, further modulating ion availability and potentially promoting a positive effect on safety by limiting the exposure of human cells to free silver ions, in line with a SbD perspetive. AgHEC also exhibited a concentration-dependent release in both media, along with a decrease in dissolution after 24 h of incubation in synthetic sweat. These non-equilibrium behaviours are likely due to the HEC coating, which can entrap Ag^+ ions on the particle surface, combined with the complexity of the medium.

AgNPs demonstrated an overall higher dissolution in synthetic sweat than in DMEM+FBS, attributable to the low pH and high chloride ion concentration, which promote the formation of soluble complexes such as AgCl, $AgCl_2^-$ and $AgCl_3^{2-}$ (Mohan et al., 2019; Tortella et al., 2020; Zanoni et al., 2021). In synthetic sweat, the dissolution reached an equilibrium, with a release of approximately 0.5 mg/L of Ag^+ that was independent of the initial nanoparticle concentration (10–50 mg/L) and the incubation time (1–24 h). In contrast, the equilibrium concentration in DMEM+FBS showed a slight dependence on the initial concentration, with approximately 0.2 mg/L and 0.1 mg/L of ions released for initial concentrations of 10 mg/L and 50 mg/L, respectively. This behavior can be attributed to the medium's complexity, where protein corona and other ligands can influence the equilibrium and the availability of free ions.

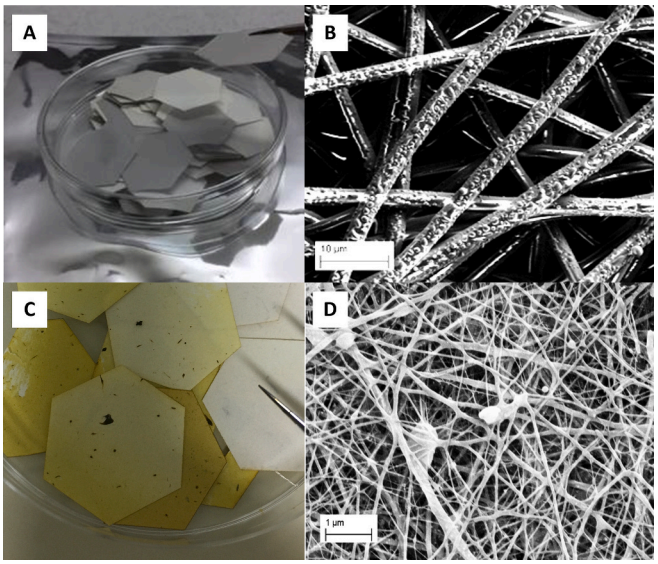

Fig. 4. Optical images and FESEM images of PLLA-Ag (A and B), and PLLA-AgHEC (C and D).

3.2. Nanosilver-enabled wound dressings

3.2.1. Morphological assessment

AgNPs and AgHEC were incorporated into PLLA fibers *via* electrospinning yielded different results (Fig. 4, Table 2). Electrospun PLLA microfibers doped with Ag showed different morphological conformations and shapes depending on the typology of embedded Ag particles. PLLA-Ag fibers presented the typical morphology of the electrospun fibers, random and nondirectional coiled with a final porous and interconnected microstructure. The diameter of the fibers was micrometric, with an average size distribution of 2.6 ± 0.4 µm (mode value 2.7), with a thickness of the electrospun layer of 50 µm and a Ag content of 5 wt% (Cazzagon et al., 2022). At higher magnification, some ridges were detected on the surface, which can be ascribed to the presence of Ag NPs. In contrast, PLLA-AgHEC fibers showed defects, secondary ramified structures, and a much smaller, broader size distribution of the diameter (62 ± 35 nm). This was likely due to an interaction between cellulose and PLLA, diluting the polymer, thereby causing a mechanical weakening.

Table 2
Ag NBMs enabled PLLA wound dressing (Cazzagon et al., 2022).

Wound dressing samples	Type of Ag	Ag Concentration on fibers (%wt)
PLLA-Ag	Uncoated	5
PLLA-AgHEC	HEC-coated	4

3.2.2. Silver release from wound dressings

As shown by the active NPs behavior, the differences in Ag release across the media can be attributed to their distinct physicochemical

characteristics, particularly pH, salt content, and ionic strength (Table 3).

The comparison between PLLA-Ag and PLLA-AgHEC fibers showed slightly higher dissolution for the PLLA-Ag patch, which contains AgNPs. The ion release measured at two points (6 and 24 h) increased over time in water for both samples, while in synthetic sweat, PLLA-AgHEC showed a reduced dissolution at 24 h. These findings are aligned with the results collected for AgHEC and are likely attributable to HEC interactions with the released ions. However, the high RSD associated with PLLA-AgHEC should be noted, due to the non-homogeneous AgHEC distribution on the patches.

To evaluate the effect of synthetic sweat on the fibers' microstructure, we examined the samples post-incubation (Fig. 5). The PLLA-Ag fibers maintained their coiled structure; however, the fiber ridges appeared altered and coated by a layer of AgCl, as confirmed by the EDX signal (Fig. S7). In contrast, the PLLA-AgHEC fibers exhibited reduced diameters and significantly diminished mechanical strength following incubation. While further optimization of the electrospinning parameters to maximize the mechanical stability of PLLA-AgHEC fibers remains possible, it was beyond the primary scope of this study. It should be noted that the immersion test in synthetic sweat represents a worst-case scenario significantly more severe than actual clinical conditions. The optimal applicability observed during the *ex-vivo* topical application on skin explants (see paragraph 3.4.1) confirms that the current fiber stability is adequate for a reliable safety and functional assessment. Consequently, further mechanical refinements are not expected to significantly alter the comparative trends reported in this study.

3.3. Evaluation of antibacterial properties

The antibacterial properties of Ag NPs and PLLA-Ag doped fibers were evaluated against *Escherichia coli* to assess the functionality of the developed NBMs (Table 4 and Table 5). *E. coli* was selected as a representative Gram-negative species due to its antibiotic resistance (Alfei and Schito, 2020), posing a grave threat to human health according to the latest WHO antibiotic resistance surveillance report (WHO Global Antimicrobial Resistance and Use System Surveillance, 2025). In solution assays, HEC alone showed antibacterial activity (94% at 400 mg/L), which decreased at the lower concentration of 40 mg/L. Both Ag-based NPs were effective at the dose of 400 mg/L. However, only AgHEC caused a total bacteria depletion at the lower concentration (Table 4). PLLA alone was inert. In contrast, both PLLA-Ag and PLLA-AgHEC displayed antibacterial activity, though only AgHEC achieved complete bacterial reduction (Table 5).

3.4. Toxicological evaluation using a porcine model

The evaluation of Ag release in relevant media for both active AgNPs and PLLA-Ag doped fibers represents the first step in supporting the overall toxicological evaluation. This evaluation was specifically conducted using two complementary porcine models supported by the innovative dOFM technique: an *in vivo* model to characterize the inflammatory response triggered by intradermal NBM delivery (Fig. 6) and an *ex vivo* model to quantify NPs penetration through the skin barrier. Porcine skin was selected for dOFM experiments due to its high anatomical and physiological similarity to human skin, including comparable epidermal thickness, follicular density, and barrier properties. This well-established model ensures clinically relevant assessment of nanoparticle penetration and local immune responses, providing a predictive bridge between *in vitro* data and human clinical outcomes (Nicolussi et al., 2025; Summerfield et al., 2015).

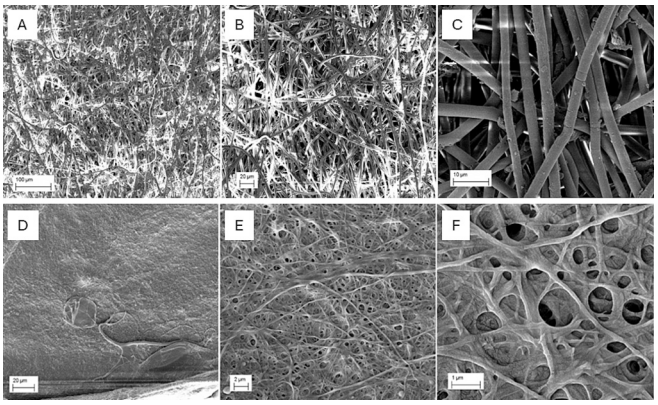

Fig. 5. FESEM images of PLLA-Ag fibers (A-C) and PLLA-AgHEC fibers (D—F) after incubation in synthetic sweat under static conditions at different magnifications. Scale bars: 100 μm (A), 20 μm (B), 10 μm (C), 20 μm (D), 2 μm (E), 1 μm (F).

Table 4
Antibacterial activity against *Escherichia coli* of HEC, AgHEC, and Ag naked NBMs at two concentrations (40 and 400 mg/L).

Samples	Bacterial reduction % (*Escherichia coli*)	
	Concentration - 400 mg/L	*Concentration - 40 mg/L*
HEC	94 ± 1	34 ± 2
AgHEC	100	100
Ag	99 ± 1	64 ± 1

Table 5
Antibacterial activity against *Escherichia coli* of PLLA, PLLA-Ag, and PLLA-AgHEC.

Samples	Bacterial reduction % (*Escherichia coli*)
PLLA	0
PLLA_Ag	95 ± 1
PLLA_AgHEC	100

3.4.1. Ex vivo study using open flow microperfusion

We used the *ex vivo* model to assess the dermal concentration of Ag after topical application of PLLA-Ag and PLLA-AgHEC in intact and disrupted skin over 24 h (refer to the Materials and methods for further details). After topical application of PLLA-Ag and PLLA-AgHEC to intact and disrupted skin for 24 h, the Ag concentration in all dOFM samples was below the limit of detection (LOD = 0.2 ng/mL). In all epidermal biopsies, Ag concentrations were higher than LOD (LOD = 6 ng/g), indicating that Ag was being released from both PLLA-Ag and PLLA-

Table 3
Ag released (%) from PLLA-Ag and PLLA-AgHEC in relevant media (synthetic sweat, and ultrapure water) at two time points (6 and 24 h).

PLLA-Ag				PLLA-AgHEC			
Time (h)	Medium	Ag released (%)	RSD (%)	Time (h)	Medium	Ag released (%)	RSD (%)
6	*Synthetic Sweat*	0.108	66	6	*Synthetic Sweat*	0.070	12
	Water	0.005	11		*Water*	0.001	52
24	*Synthetic Sweat*	0.183	42	24	*Synthetic Sweat*	0.031	41
	Water	0.010	18		*Water*	0.011	34

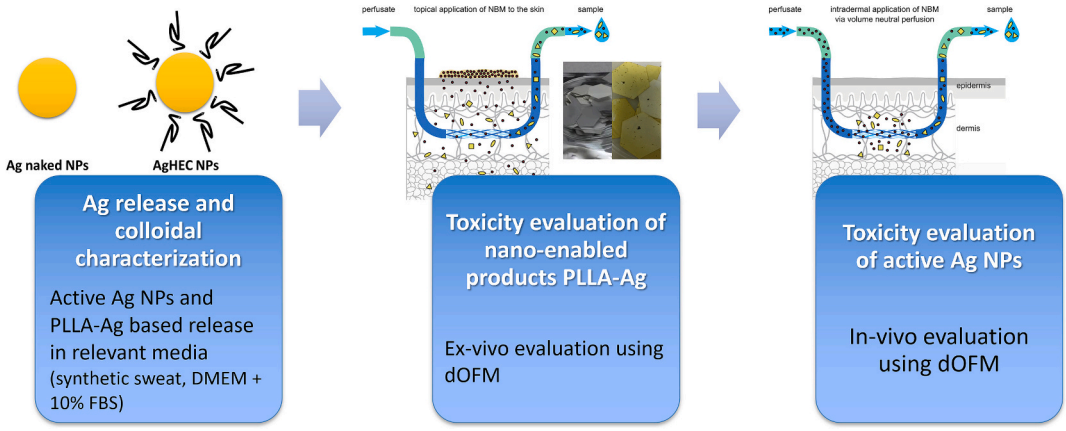

Fig. 6. Scheme of the multi-tiered toxicological assessment of the Ag NPs and PLLA-Ag-based NBMs.

AgHEC. In dermal biopsies, Ag concentration was above LOD in only 3 of 9 biopsies for PLLA-Ag, and in 4 of 9 biopsies for PLLA-AgHEC. Ag concentrations in biopsies were similar after the topical application of PLLA-Ag and PLLA-AgHEC in epidermis and dermis (Fig. 7). The low concentration in both dOFM samples and dermal biopsies showed that there was a low skin penetration of Ag after applying PLLA-Ag and PLLA-AgHEC directly to the skin. We assume that the Ag concentration in biopsies was higher than in the dOFM samples because biopsies included more superficial skin tissue, in which the Ag concentration was higher.

3.4.2. *In vivo study using open flow microperfusion*

Although we observed Ag concentrations above or below the expected range in the *in vitro* adsorption test (Supplementary Information), we determined that NBM concentrations were sufficiently high to proceed with the *in vivo* study. Cytokine secretion was determined as a measure of the immune response (Elsabahy and Wooley, 2013). Specifically, the proinflammatory cytokines, TNF-α, IL-6, and IL-8 (a member of the C-X-C motif subfamily of chemokines, also known as CXCL8), and the anti-inflammatory cytokine, IL-10 were evaluated by ELISA. We found that IL-6, IL-8, and TNF-α concentrations increased over 12 h during intradermal delivery of Ag, AgHEC, and the negative control (no NBM) while the IL-10 concentration remained constant (Fig. 8). There were no significant differences in the area under the curve (AUC) of IL-6, IL-8, IL-10, and TNF-α between Ag and AgHEC and the control site (all p-values >0.36, Fig. 9). However, the expression levels

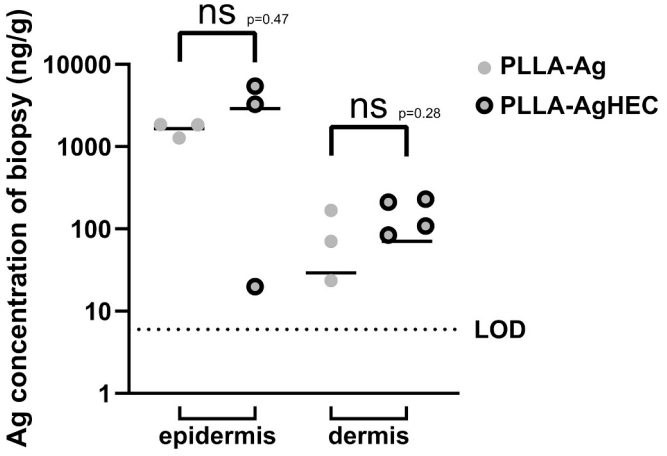

Fig. 7. Ag concentration in biopsies of epidermis and dermis 24 h after topical application of PLLA-Ag and PLLA-AgHEC. Horizontal line: mean value; Horizontal dotted line: limit of detection (LOD); not significant (ns). To calculate mean values, concentrations of Ag below the LOD were assumed to be zero.

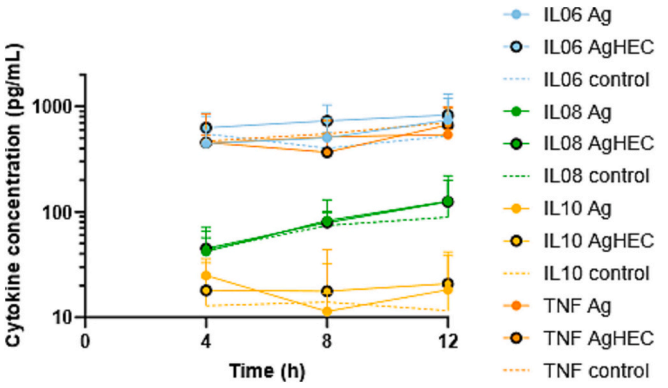

Fig. 8. Concentration-time profiles of the cytokines IL-6, IL-8, IL-10, and TNF-α in the dermis over 12 h of intradermal delivery of Ag, AgHEC, and no NBMs (control) *via* dOFM probes. Each data point represents the mean concentrations of one sampling interval (4 h, $N = 4$). The data points are shown at the end of each interval.

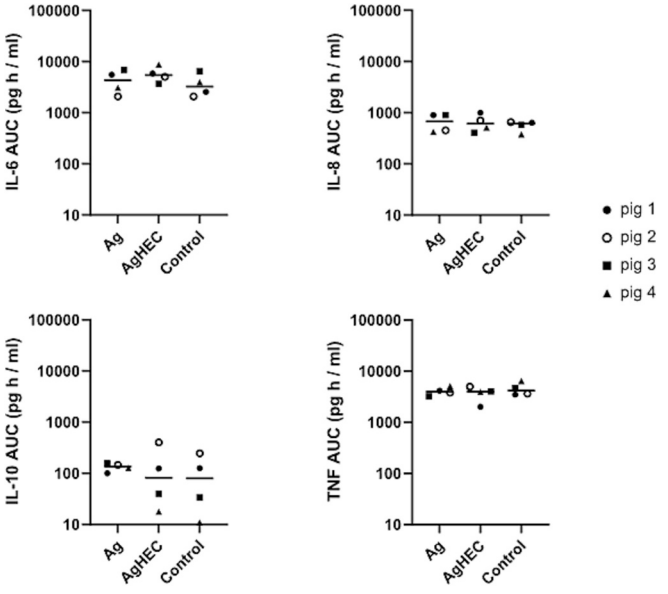

Fig. 9. Expression of IL-6, IL-8, IL-10, and TNF-α plotted as AUC values in the dermis over 12 h of intradermal delivery of Ag, AgHEC, and no NBMs (control) *via* dOFM probe. Horizontal lines represent the mean values.

of IL-6, IL-8, IL-10, and TNF-α differed. Hence, IL-6 and TNF-α showed the highest concentrations with a mean of 594.3 ± 319.9 pg/mL (IL-6) and 523.8 ± 221.3 pg/mL (TNF), followed by IL-8 (78.5 ± 52.6 pg/mL) and IL-10 (16.6 ± 15.3 pg/mL). Surface coatings of NPs may also drive immune responses (Bi et al., 2023; Ilinskaya and Dobrovolskaia, 2016). However, we could not observe significant differences between uncoated Ag and AgHEC (Fig. 8, Fig. 9).

Ag concentrations were also determined. After 12 h of intradermal delivery, the Ag concentrations at the Ag biopsy sites were 2630 ± 3638 ng/g at 0 mm distance and 125 ± 109 ng/g at 2 mm, and for AgHEC 9848 ± 7300 ng/g at 0 mm and 1146 ± 1229 pg/g at 2 mm. Since Ag was found in the biopsies, we can assume that it was delivered intradermally with the dOFM. Although not significant, the mean Ag concentration showed a tendency to be higher for AgHEC than for the Ag NPs both at 0 mm ($p = 0.13$) and at 2 mm ($p = 0.15$) (Fig. 10A). However, we found no difference when looking at the relative change in concentration from 0 mm to 2 mm, comparing Ag and AgHEC ($p = 0.99$) (Fig. 10B). This indicates that the diffusion rate in the tissue was the same for Ag and AgHEC.

4. Conclusions

In this study, we presented a targeted safety and efficacy assessment of a hydroxyethyl cellulose-coated silver nanoparticle (AgHEC) and its integration into PLLA-based wound dressings, in comparison to conventional, uncoated AgNPs. Through a multi-tiered approach that combined advanced physicochemical characterization with innovative biological models, we evaluated the functional and toxicological profile of these NBMs throughout their use phase as wound care products. Our findings confirm that the AgHEC formulation offers an improved antibacterial efficacy compared to its uncoated counterpart. Most importantly, the toxicological evaluation using state-of-the-art porcine skin models and dermal open flow microperfusion (dOFM) provided critical insights. The *ex vivo* model demonstrated negligible penetration of silver through both intact and disrupted skin over 24 h following the topical application of the PLLA-Ag and PLLA-AgHEC dressings. Ag penetration through skin barrier was low at 24 h after topical application of PLLA-Ag and PLLA-AgHEC. Ag concentrations in dOFM samples were below 0.2 ng/mL, 24 h after topical application. Furthermore, the *in vivo* model revealed that the direct intradermal delivery of both Ag and AgHEC nanoparticles did not elicit a significant or elevated inflammatory immune response compared to the control. The rate of diffusion in the dermis was similar for Ag and AgHEC. Delivering NBMs locally to skin tissue *via* dOFM allowed us to simultaneously monitor immune response biomarkers, providing a detailed insight into comprehensive understanding of NBM-skin interactions. This integrated workflow provides evidence that supports the safety of the developed nanosilver-enabled wound dressings. The combination of potent antibacterial activity with a lack of significant dermal penetration or local inflammatory response indicates that the risk of topical toxicity from these materials is low. Therefore, this work not only underlines AgHEC as a promising SbD alternative for wound healing applications but also offers a contribution to the safety evaluation within the scope of the SSbD approach for the future evaluation of NBMs, showcasing the utility of the open flow microperfusion system.

CRediT authorship contribution statement

Ilaria Zanoni: Writing – original draft, Visualization, Investigation. **Simon Schwingenschuh:** Writing – review & editing, Investigation. **Thomas Birngruber:** Validation, Data curation. **Peter Reisenegger:** Investigation. **Sandeep Keshavan:** Methodology, Investigation. **Sebastian Santhosh Martin:** Investigation. **Bengt Fadeel:** Writing – review & editing, Investigation. **Kai Moritz Eder:** Investigation. **Jürgen Schnekenburger:** Methodology. **Alessandro Bonetto:** Methodology, Investigation. **Elena Badetti:** Writing – review & editing, Data curation.

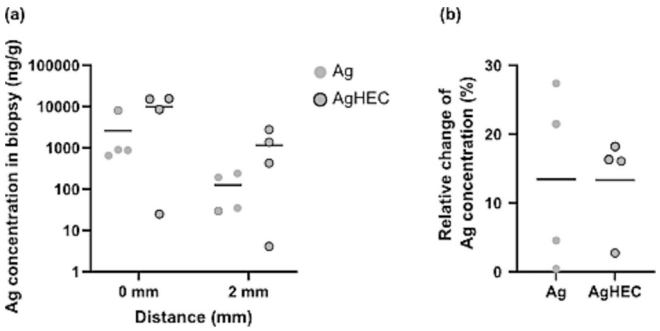

Fig. 10. Ag concentrations as a marker of dermal penetration. (A) Ag concentration in skin biopsies 12 h after the start of intradermal delivery of Ag and AgHEC *via* dOFM probes. The distance is the distance between center of the dOFM probe and center of the biopsy. (B) Ag concentration at distance 2 mm normalized to the initial concentration at distance 0 mm. Horizontal lines in (A) and (B) represent mean values.

Claudia Vineis: Methodology. **Simona Ortelli:** Data curation. **Anna Luisa Costa:** Writing – review & editing, Visualization. **Magda Blosi:** Writing – review & editing, Writing – original draft, Visualization, Conceptualization.

Declaration of competing interest

The authors declare that they have no known competing financial interests or personal relationships that could have appeared to influence the work reported in this paper.

Acknowledgments

This work was supported by the European Union's Horizon 2020 Research and Innovation Programme through BIORIMA (Biomaterials Risk Management) (Grant Agreement No. 760928) (Coordinator: Prof. Lang Tran). The authors wish to acknowledge Dr. Anne Marzi for her contribution to the endotoxin determination within the BIORIMA project.

Appendix A. Supplementary data

Supplementary data to this article can be found online at https://doi.org/10.1016/j.impact.2026.100630.

Data availability

Data will be made available on request.

References

Albalghiti, E., Stabryla, L.M., Gilbertson, L.M., Zimmerman, J.B., 2021. Towards resolution of antibacterial mechanisms in metal and metal oxide nanomaterials: a meta-analysis of the influence of study design on mechanistic conclusions. Environ. Sci. Nano 8, 37–66. https://doi.org/10.1039/D0EN00949K.

Alfei, S., Schito, A.M., 2020. Positively charged polymers as promising devices against multidrug resistant gram-negative bacteria: a review. Polymers (Basel). 12. https://doi.org/10.3390/POLYM12051195.

Bi, J., Mo, C., Li, S., Huang, M., Lin, Y., Yuan, P., Liu, Z., Jia, B., Xu, S., 2023. Immunotoxicity of metal and metal oxide nanoparticles: from toxic mechanisms to metabolism and outcomes. Biomater. Sci. 11, 4151–4183. https://doi.org/10.1039/D3BM00271C.

Birngruber, T., Tiffner, K.I., Mautner, S.I., Sinner, F.M., 2022. Dermal open flow microperfusion for PK-based clinical bioequivalence studies of topical drug products. Front. Pharmacol. 13, 1–7. https://doi.org/10.3389/fphar.2022.1061178.

Blosi, M., Brigliadori, A., Ortelli, S., Zanoni, I., Gardini, D., Vineis, C., Varesano, A., Ballarin, B., Perucca, M., Costa, A.L., 2024. Re-designing nano-silver technology exploiting one-pot hydroxyethyl cellulose-driven green synthesis. Front. Chem. 12, 1–15. https://doi.org/10.3389/fchem.2024.1432546.

Bodenlenz, M., Tiffner, K.I., Raml, R., Augustin, T., Dragatin, C., Birngruber, T., Schimek, D., Schwagerle, G., Pieber, T.R., Raney, S.G., Kanfer, I., Sinner, F., 2017.

Open flow microperfusion as a dermal pharmacokinetic approach to evaluate topical bioequivalence. Clin. Pharmacokinet. 56, 91–98. https://doi.org/10.1007/s40262-016-0442-z.
Booth, A., Alstrup Jensen, K., 2015. SOP for probe sonicator calibration of delivered acoustic power and de-agglomeration efficiency for ecotoxicological testing. NANoREG.
Caldeira, C., Farcal, R., Garmendia Aguirre, I., Mancini, L., Tosches, D., Amelio, A., Rasmussen, K., Rauscher, H., Riego Sintes, J., Sala, S., 2022. Safe and sustainable by design chemicals and materials - framework for the definition of criteria and evaluation procedure for chemicals and materials. Publications Office of the European Union. https://doi.org/10.2760/487955.
Caldeira, C., Abbate, E., Moretti, C., Mancini, L., Sala, S., 2024. Safe and sustainable chemicals and materials: a review of sustainability assessment frameworks. Green Chem. 26, 7456–7477. https://doi.org/10.1039/D3GC04598F.
Cassa, M.A., Gentile, P., Girón-Hernández, J., Ciardelli, G., Carmagnola, I., 2024. Smart self-defensive coatings with bacteria-triggered antimicrobial response for medical devices. Biomater. Sci. 12, 5433–5449. https://doi.org/10.1039/d4bm00936c.
Cazzagon, V., Giubilato, E., Bonetto, A., Blosi, M., Zanoni, I., Costa, A.L., Vineis, C., Varesano, A., Marcomini, A., Hristozov, D., Semenzin, E., Badetti, E., 2022. Identification of the safe(r) by design alternatives for nanosilver-enabled wound dressings. Front. Bioeng. Biotechnol. 10. https://doi.org/10.3389/fbioe.2022.987650.
Chaturvedi, S., Garg, A., 2021. An insight of techniques for the assessment of permeation flux across the skin for optimization of topical and transdermal drug delivery systems: “modelling the topical and transdermal drug delivery systems.”. J. Drug Delivery Sci. Technol. 62, 102355. https://doi.org/10.1016/j.jddst.2021.102355.
Ciofu, O., Rojo-Molinero, E., Macià, M.D., Oliver, A., 2017. Antibiotic treatment of biofilm infections. Apmis 125, 304–319. https://doi.org/10.1111/apm.12673.
Costa, A.L., Blosi, M., 2016. WO2016125070A1.
Costa, A.L., Blosi, M., Brigliadori, A., Zanoni, I., Ortelli, S., Simeone, F.C., Delbue, S., D'Alessandro, S., Parapini, S., Vineis, C., Varesano, A., Toprak, M.S., Hamawandi, B., Gardini, D., 2022. Eco design for ag-based solutions against SARS-CoV-2 and e. coli. Environ. Sci. Nano 9, 4295–4304. https://doi.org/10.1039/d2en00178k.
Crosera, M., Bovenzi, M., Maina, G., Adami, G., Zanette, C., Florio, C., Filon Larese, F., 2009. Nanoparticle dermal absorption and toxicity: a review of the literature. Int. Arch. Occup. Environ. Health 82, 1043–1055. https://doi.org/10.1007/s00420-009-0458-x.
Dhivya, S., Padma, V.V., Santhini, E., 2015. Wound dressings - a review. Biomed 5, 24–28. https://doi.org/10.7603/s40681-015-0022-9.
Doorley, G.W., Payne, C.K., 2011. Cellular binding of nanoparticles in the presence of serum proteins. Chem. Commun. 47, 466–468. https://doi.org/10.1039/c0cc02618b.
Eder, K.M., Marzi, A., Barroso, Á., Ketelhut, S., Kemper, B., Schnekenburger, J., 2022. Label-free digital holographic microscopy for in vitro cytotoxic effect quantification of organic nanoparticles. Cells. https://doi.org/10.3390/cells11040644.
Elsabahy, M., Wooley, K.L., 2013. Cytokines as biomarkers of nanoparticle immunotoxicity. Chem. Soc. Rev. 42, 5552–5576. https://doi.org/10.1039/C3CS60064E.
Furxhi, I., Perucca, M., Blosi, M., Lopez de Ipiña, J., Oliveira, J., Murphy, F., Costa, A.L., 2022. ASINA project: towards a methodological data-driven sustainable and safe-by-design approach for the development of nanomaterials. Front. Bioeng. Biotechnol. 9, 1–8. https://doi.org/10.3389/fbioe.2021.805096.
Furxhi, I., Perucca, M., Koivisto, A.J., Bengalli, R., Mantecca, P., Nicosia, A., Burrueco-Subirà, D., Vázquez-Campos, S., Lahive, E., Blosi, M., de Ipiña, J.L., Oliveira, J., Carriere, M., Vineis, C., Costa, A., 2024. A roadmap towards safe and sustainable by design nanotechnology: implementation for nano-silver-based antimicrobial textile coatings production by ASINA project. Comput. Struct. Biotechnol. J. 25, 127–142. https://doi.org/10.1016/j.csbj.2024.06.013.
Gabrielsson, J., Weiner, D., 2012. Non-compartmental analysis - chapter 16. In: Methods in Molecular Biology (ed.), Computational Toxicology. springer science+business media, pp. 377–389. https://doi.org/10.1007/978-1-62703-050-2.
Garmendia Aguirre, I., Abbate, E., Bracalente, G., Mancini, L., Cappucci, G.M., Tosches, D., Rasmussen, K., Sokull-Kluettgen, B., Rauscher, H., Sala, S., 2025. Safe and Sustainable by Design Chemicals and Materials. Revised framework. Publications Office of the European Union, Luxembourg. https://doi.org/10.2760/5103785.
Giubilato, E., Cazzagon, V., Amorim, M.J.B., Blosi, M., Bouillard, J., Bouwmeester, H., Costa, A.L., Fadeel, B., Fernandes, T.F., Fito, C., Hauser, M., Marcomini, A., Nowack, B., Pizzol, L., Powell, L., Prina-Mello, A., Sarimveis, H., Scott-Fordsmand, J. J., Semenzin, E., Stahlmecke, B., Stone, V., Vignes, A., Wilkins, T., Zabeo, A., Tran, L., Hristozov, D., 2020. Risk management framework for nano-biomaterials used in medical devices and advanced therapy medicinal products. Materials (Basel). 13, 1–29. https://doi.org/10.3390/ma13204532.
Ilinskaya, A.N., Dobrovolskaia, M.A., 2016. Understanding the immunogenicity and antigenicity of nanomaterials: past, present and future. Toxicol. Appl. Pharmacol. 299, 70–77. https://doi.org/10.1016/j.taap.2016.01.005.
Jensen, K.A., 2014. The NANOGENOTOX Dispersion Protocol for NANoREG. Nrcwe.
Jude, E.B., Apelqvist, J., Spraul, M., Martini, J., Jones, G., Harding, K., Benbow, S., Young, M., Malik, R., O'Brien, I., Charpentier, G., Vigier-Simorre, N., Le Devehat, C., Richard, L., Vanscheidt, W., Muenter, C., Baer, M., 2007. Prospective randomized controlled study of hydrofiber® dressing containing ionic silver or calcium alginate dressings in non-ischaemic diabetic foot ulcers. Diabet. Med. 24, 280–288. https://doi.org/10.1111/j.1464-5491.2007.02079.x.
Larese Filon, F., D'Agostin, F., Crosera, M., Adami, G., Renzi, N., Bovenzi, M., Maina, G., 2009. Human skin penetration of silver nanoparticles through intact and damaged skin. Toxicology 255, 33–37. https://doi.org/10.1016/j.tox.2008.09.025.
Larese Filon, F., Mauro, M., Adami, G., Bovenzi, M., Crosera, M., 2015. Nanoparticles skin absorption: new aspects for a safety profile evaluation. Regul. Toxicol. Pharmacol. 72, 310–322. https://doi.org/10.1016/j.yrtph.2015.05.005.
Maeda, N., Jiao, H., Kłosowska-Chomiczewska, I.E., Artichowicz, W., Preiss, U., Szumała, P., Macierzanka, A., Jungnickel, C., 2025. Nanoparticle skin penetration: depths and routes modeled in-silico. Small 21, 2412541. https://doi.org/10.1002/smll.202412541.
Marassi, V., Di Cristo, L., Smith, S.G.J., Ortelli, S., Blosi, M., Costa, A.L., Reschiglian, P., Volkov, Y., Prina-Mello, A., 2018. Silver nanoparticles as a medical device in healthcare settings: a five-step approach for candidate screening of coating agents. R. Soc. Open Sci. 5. https://doi.org/10.1098/rsos.171113.
Martin, S., de Haan, L., Miro Estruch, I., Eder, K.M., Marzi, A., Schnekenburger, J., Blosi, M., Costa, A., Antonello, G., Bergamaschi, E., Riganti, C., Beal, D., Carrière, M., Taché, O., Hutchison, G., Malone, E., Young, L., Campagnolo, L., La Civita, F., Pietroiusti, A., Devineau, S., Baeza, A., Boland, S., Zong, C., Ichihara, G., Fadeel, B., Bouwmeester, H., 2022. Pre-validation of a reporter gene assay for oxidative stress for the rapid screening of nanobiomaterials. Front. Toxicol. 4.
Mohan, S., Princz, J., Ormeci, B., DeRosa, M.C., 2019. Morphological transformation of silver nanoparticles from commercial products: modeling from product incorporation, weathering through use scenarios, and leaching into wastewater. Nanomaterials 9. https://doi.org/10.3390/nano9091258.
Nicolussi, P., Pilo, G., Cancedda, M.G., Peng, G., Chau, N.D.Q., De la Cadena, A., Vanna, R., Samad, Y.A., Ahmed, T., Marcellino, J., Tedde, G., Giro, L., Ylmazer, A., Loi, F., Carta, G., Secchi, L., Dei Giudici, S., Macciocu, S., Polli, D., Nishina, Y., Ligios, C., Cerullo, G., Ferrari, A., Bianco, A., Fadeel, B., Franzoni, G., Delogu, L.G., 2025. Biocompatibility of water-dispersible pristine graphene and graphene oxide using a close-to-human animal model: a pilot study on swine. Adv. Healthc. Mater. 14, 2401783. https://doi.org/10.1002/adhm.202401783.
OECD, 2002. Test no. 308: aerobic and anaerobic transformation in aquatic sediment system. In: OECD Guidel. Test. Chem., 19. https://doi.org/10.1787/9789264070523-en.
Paladini, F., Pollini, M., 2019. Antimicrobial silver nanoparticles for wound healing application: Progress and future trends. Materials (Basel). 12. https://doi.org/10.3390/ma12162540.
Percival, S.L., McCarty, S.M., 2015. Silver and alginates: role in wound healing and biofilm control. Adv. Wound Care 4, 407–414. https://doi.org/10.1089/wound.2014.0541.
Pieber, T., Birngruber, T., Bodenlenz, M., Höfferer, C., Mautner, S., Tiffner, K., Sinner, F., 2013. Open flow microperfusion: an alternative method to microdialysis? Microdialysis. Drug Dev. 283–302.
Shi, C., Wang, C., Liu, H., Li, Q., Li, R., Zhang, Y., Liu, Y., Shao, Y., Wang, J., 2020. Selection of appropriate wound dressing for various wounds. Front. Bioeng. Biotechnol. 8, 1–17. https://doi.org/10.3389/fbioe.2020.00182.
Summerfield, A., Meurens, F., Ricklin, M.E., 2015. The immunology of the porcine skin and its value as a model for human skin. Mol. Immunol. 66, 14–21. https://doi.org/10.1016/j.molimm.2014.10.023.
Tak, Y.K., Pal, S., Naoghare, P.K., Rangasamy, S., 2015. Shape-dependent skin penetration of silver nanoparticles: does it really matter ? Nat. Publ. Gr. 1–11. https://doi.org/10.1038/srep16908.
Tortella, G.R., Rubilar, O., Durán, N., Diez, M.C., Martínez, M., Parada, J., Seabra, A.B., 2020. Silver nanoparticles: toxicity in model organisms as an overview of its hazard for human health and the environment. J. Hazard. Mater. 390, 121974. https://doi.org/10.1016/J.JHAZMAT.2019.121974.
Von Goetz, N., Lorenz, C., Windler, L., Nowack, B., Heuberger, M., Hungerbühler, K., 2013. Migration of ag- and TiO2-(nano)particles from textiles into artificial sweat under physical stress: experiments and exposure modeling. Environ. Sci. Technol. 47, 9979–9987. https://doi.org/10.1021/es304329w.
WHO Global Antimicrobial Resistance and Use System Surveillance, 2025. Global antibiotic resistance surveillance report 2025.
Wu, K., Li, H., Cui, X., Feng, R., Chen, W., Jiang, Y., Tang, C., Wang, Yaohai, Wang, Yan, 2022. Mutagenesis and resistance development of bacteria. Antimicrob. Agents Chemother. 66.
Yetisen, A.K., Qu, H., Manbachi, A., Butt, H., Dokmeci, M.R., Hinestroza, J.P., Skorobogatiy, M., Khademhosseini, A., Yun, S.H., 2016. Nanotechnology in textiles. ACS Nano 10, 3042–3068. https://doi.org/10.1021/acsnano.5b08176.
Zanoni, I., Crosera, M., Pavoni, E., Adami, G., Mauro, M., Costa, A.L., Lead, J.R., Larese Filon, F., 2021. Use of single particle ICP-MS to estimate silver nanoparticle penetration through baby porcine mucosa. Nanotoxicology 15, 1005–1015. https://doi.org/10.1080/17435390.2021.1940338.